Electrochimica Acta 54 (2009) 7201–7206

Contents lists available at ScienceDirect

Electrochimica Acta

journal homepage: www.elsevier.com/locate/electacta

Sonoelectrochemical (20 kHz) production of platinum nanoparticles from aqueous solutions

Valentina Zin[a], Bruno G. Pollet[b,*], Manuele Dabalà[a]

[a] DPCI – University of Padua, via Marzolo, 9, 35131 Padova, Italy
[b] Fuel Cells Group, School of Chemical Engineering, The University of Birmingham, Edgbaston Road, Edgbaston, Birmingham B15 2TT, UK

ARTICLE INFO

Article history:
Received 25 February 2009
Received in revised form 22 May 2009
Accepted 1 July 2009
Available online 9 July 2009

Keywords:
Platinum
Nanoparticles
Sonoelectrode
Power ultrasound
Sonochemistry

ABSTRACT

The present work describes the production of platinum nanoparticles from aqueous chloroplatinic solutions in the presence of low-frequency high-power ultrasound (20 kHz) on titanium alloy electrodes. The production of this new type of Pt nanoparticles was performed galvanostatically at (298 ± 1) K using a newly designed experimental set-up and '*sonoelectrode*' producing ultrasonic pulses triggered and followed immediately by short applied current pulses. From galvanostatic studies, it was shown that Pt mean grain size ranging from 11 to 15 nm was produced. Morphological and structural studies of the produced nanoparticles were performed by TEM, SEM, XRD and SAED and showed that Pt nanoaggregates were predominantly formed, with no redissolution of the nanoaggregates. Globular clusters had a mean size ranging between 100 and 200 nm which in turn aggregated and built complex structures.

1. Introduction

The use of ultrasound on electrochemical systems or Sonoelectrochemistry was first observed by Moriguchi as early as 1934 [1] and continues to be an active and exciting research area [2]. Extensive work has been carried out in which high power ultrasound was applied to various electrochemical processes leading to several industrial applications and many publications over a wide range of subject areas such as electrodeposition, electroplating, electrochemical dissolution and corrosion testing.

It was shown that the effects of high intensity ultrasonic irradiation on electrochemical processes lead to both chemical and physical effects, for example, mass-transport enhancement, surface cleaning and radical formation. Many workers have also investigated the distribution of ultrasonic waves or energy in various electrochemical reactors operating in the lower ultrasonic frequency range (20–100 kHz) and at high ultrasonic powers. Several methods for such determination have been proposed, e.g. aluminum foil erosion, sonoluminescence, calorimetric methods, chemical dosimetry [2] and laser-sheet visualization [3].

Many of the observed effects in Sonoelectrochemistry may be explained by the enhancement of mass-transport in diffusion-controlled processes. The extensive work of Coury and co-worker [4] and Compton et al. [5,6] were probably the first "modern" examples investigating mass transfer phenomena under sonication. Power ultrasound is known to decrease the diffusion layer thickness (δ) thereby giving substantial increase in limiting current (I_{lim}) attributed due to effects of cavitation and/or micro- and macro-streaming. It is known in the field that both cavitational and acoustic streaming effects contribute significantly to the increase in observed experimental currents [4–7]. The experimental decrease in the diffusion layer thickness is also known to be due to asymmetrical collapse of cavitation bubbles at the electrode surface leading to the formation of high velocity jets of liquid being directed toward its surface. This jetting, together with acoustic streaming, is thought to lead to random punctuation and disruption of the mass transfer boundary layer at the electrode surface at close electrode-to-horn separations. Birkin et al. [8,9] also showed that the nature of the solvent is paramount in assigning limiting currents. More recently, Pollet et al. [10] showed, with aid of mathematical models based on mass-balance equations, that a Levich-like equation relating the limiting current density, the square root of ultrasonic intensity and the inverse square root of the electrode–horn distance, may be generated for ultrasonic frequencies of 20 and 40 kHz allowing the generation of an 'equivalent' flow velocity under sonication, an important and useful parameter in chemical engineering.

Recently, an upsurge of interests has been observed in the synthesis of metallic nanoparticles [11–13]. In the last decade, the production of metallic platinum nanoparticles has been investigated as they offer high surface-to-volume ratios and have considerable potential for usage in various areas such as fuel cells, reforming, catalysis and medicine [14,15]. There are a range

* Corresponding author. Tel.: +44 781 495 2112; fax: +44 121 414 5377.
E-mail address: b.g.pollet@bham.ac.uk (B.G. Pollet).

0013-4686/$ – see front matter © 2009 Elsevier Ltd. All rights reserved.
doi:10.1016/j.electacta.2009.07.001

of methods of producing metallic platinum nanosized materials including thermal decomposition, physical and thermal evaporation, laser ablation, laser-assisted catalytic growth (LCG), vapor–liquid–solid growth (VLS), ultrahigh-vacuum (UHV), ion implantation, biochemical, electrochemical, sonochemical, radiolysis, chemical reduction/oxidation and sol–gel [15]. However, most of these techniques tend to be expensive and time-consuming. An alternative method, which is both simple and cost-effective, is the use of Sonoelectrochemistry. For example, based on the original work of Reisse et al. [16,17] for the production of copper, Dabalà and Pollet [18] produced for the first time nanosized Fe–Co metallic particles sonoelectrochemically, in which the ultrasonic horn was used as the working electrode. This '*sonoelectrode*' was subjected to ultrasonic pulses which were each followed by short applied current pulses. They showed that, during cavitation, a jet of liquid penetrates inside the cavitation bubble perpendicular to the '*sonoelectrode*' surface and the resulting impact was responsible for dislodging any nanopowder material which had been electrochemically deposited on the surface.

This paper reports for the first time, a study on the synthesis of platinum nanoparticles by using the new method combining metallic electrodeposition with low-frequency high-power ultrasound (20 kHz). In this study the platinum nanopowders produced were characterized both morphologically and chemically.

2. Experimental

The apparatus employed for the production of platinum nanosized materials was similar to that employed by Reisse et al. and Pollet and Dabalà [17,18] [Fig. 1(a)]. The system consisted of a two-electrode set-up, namely (i) a titanium alloy (Ti–6Al–4V) horn acting both as the cathode and the ultrasonic emitter (described therein as the *sonoelectrode*) linked to a AMEL 7060 potentiostat operating in galvanostatic mode and a 20 kHz ultrasonic generator (Sintec Generator EG36) and (ii) a platinum mesh acting as the anode linked to the potentiostat. Electrochemical experiments were performed using a cylindrical vessel (200 ml) [Fig. 1(a)]. The electrochemical cell was placed in a Faraday cage. Temperature was regulated by a glass cooling coil (C) placed inside the electrochemical cell and linked to a thermostatted bath operating at preset temperatures. The temperature of the electro-analyte was measured with a Fluke 51 digital thermometer fitted to a K-type thermocouple. A heat-shrinkable sleeve surrounded the side walls of the extreme part of the sonoelectrode, leaving only a flat active surface for the electrodeposition equal to 1.227 cm^2 (ultrasonic horn tip area determined coulometrically) [Fig. 1(a)]. A constant galvanostatic current was applied to the sonoelectrode and the maximum ultrasonic power ultrasound employed was 76 W. A trigger acted like a switch with the role of closing alternatively the circuits in which the potentiostat and the piezoelectric power supply operated. The pulse drivers allowed applied galvanic current and ultrasonic pulsing.

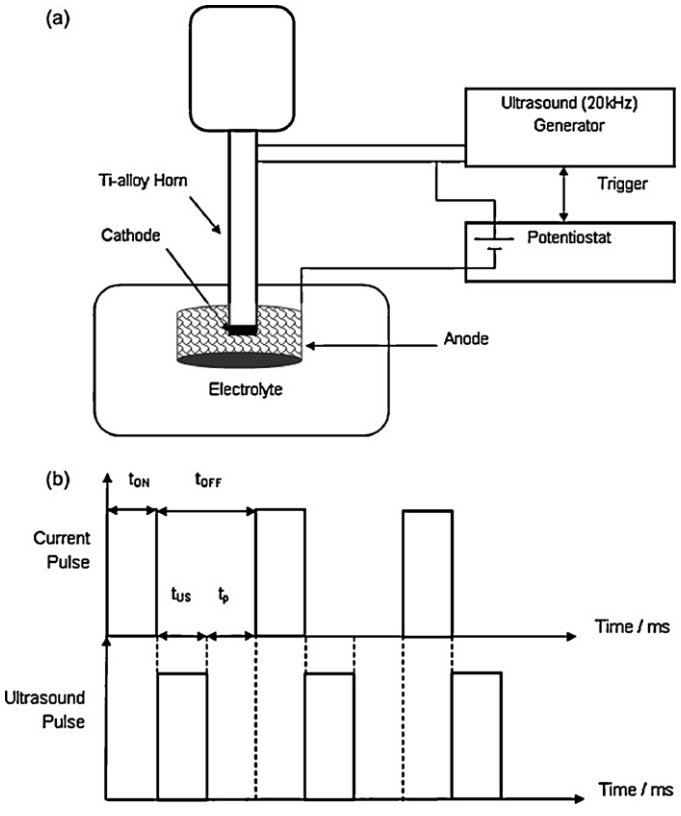

Fig. 1. (a) Schematic of the sonoelectrochemical nanoparticle production setup and (b) time management for Pt sonoelectrosyntheses.

All electrodes were electrochemically cleaned by cycling in sulphuric acid (1.0 mol dm^{-3}) for 10 min prior to the experiments. They were then washed with high quality MilliQ water and all Ti electrodes were polished to a mirror finish first with grinding paper (Buelher-Met, P600) and then sequentially with 25 μm down to 0.3 μm alumina oxide paste and were cleaned with immersion in nitric acid for 5 min in order to remove any traces of contaminants.

For the production of nanopowders, the time management sequence employed was as follows [Fig. 1(b)]:

1. A short current pulse of $|i| = 50$ mA cm^{-2} was applied to the *sonoelectrode*, and here the titanium horn acted as an electrode only (t_{ON}); the time of this phase typically varied between 0.3 and 0.5 s.
2. Immediately after the electrochemical pulse was turned off, an ultrasonic pulse was sent to the *sonoelectrode* and here it acted only as a vibrating ultrasonic horn (t_{US}); this second phase lasted no more than 0.5 s.
3. A rest time, t_p, followed the two previous phases (this was useful to restore the initial electrolyte conditions close to the *sonoelectrode*).

A characteristic time management parameter of the process, χ, was employed according to Eq. (1) [17,18]:

$$\chi = \frac{t_{ON}}{t_{ON} + t_{OFF}} \quad (1)$$

where $t_{OFF} = t_{US} + t_p$

By controlling the varying process parameter, χ, and the applied current, it was possible to produce sonoelectrochemically high purity and high surface/volume ratio suspended nanoparticles which were filtered with 0.05 μm Millipore filters under vacuum.

The filters were then washed with pure ethanol, dried for 48 h in a silica-gel drier and stored under vacuum. Each filter was weighted after dehydration and the efficiency of the process was calculated as the ratio of the produced mass of powder to the faradic yield according to Eq. (2) [19]:

$$m_f = \frac{\chi \cdot I \cdot t}{F} \cdot \frac{\sum_i (x_i \cdot PA_i)}{\sum_i (x_i \cdot n_{ei})} \quad (2)$$

where χ is $t_{ON}/(t_{ON} + t_{OFF})$, I is the applied current in A, t is the total time in s, F is the Faraday constant (96,500 C mol^{-1}), x_i is the molar fraction, PA_i is the atomic weight of Pt in g mol^{-1} (195.09 g mol^{-1}) and n_{ei} is the number of electron transferred (=2).

Table 1
Cathode efficiency (η) of Pt nanoparticles showing variation of time management. t_{ON} (s) is the applied current pulse time (s); t_{US} (s) is the applied ultrasonic pulse time (s); t_p is the rest time (s); χ (chi) is the varying process parameter; m_f is the faradic yield (mg); m_r is the actual yield (mg); η is the cathode efficiency (%).

Test #	t_{ON}/s	t_{US}/s	t_r/s	χ	η/%
1	0.2	0.5	0.2	0.222	67.5
2	0.2	0.3	0.2	0.2857	80.5
3	0.3	0.5	0.2	0.3	59.3
4	0.3	0.3	0.2	0.375	83.4
5	0.5	0.3	0.2	0.5	73.8

For each run, the cathode efficiency, η in % was determined using Eq. (3) [20]:

$$\eta = \frac{m_r}{m_f} \cdot 100\% \quad (3)$$

where m_f is the faradaic yield in g and m_r is the actual metallic mass produced during the sonoelectrochemical tests in g.

The produced powders were analyzed by X-EDS (Philips EDAX PV9800) in views of identifying any contaminant. Morphological studies of the Pt nanopowders were performed on both a scanning electron microscope (Stereoscan 440 SEM, Cambridge, equipped with a Philips EDAX PV9800) and a transmission electron microscope (JEOL 2000FX operating at 160 kV). X-ray diffractometer (Siemens D500 XRD) with Cu K_α radiation (λ = 1.5418 Å, 40 kV and 30 mA) was used for the identification of the phases and the measurement of grain size in the powders. $2\theta/\theta$ diffractograms were obtained in the 35–85° range with a step of 0.03° with a measuring time of 15 s per step.

Finally, for all experiments, chemical reagents were of AnalaR grade or equivalent. All Pt nanopowders were synthesized from a chloride bath. Aqueous chloroplatinic solutions of 0.1 mol dm^{-3} K_2PtCl_4 and 0.5 mol dm^{-3} NaCl (background electrolyte) were freshly prepared using high quality MilliQ water (R = 12 MΩ). The pH (1 ± 0.1) of the chloroplatinic solutions was measured before and after each experiments and showed no variations from the value set at the start. Ultrasonic powers were determined calorimetrically using the method of Margulis et al. [21,22] and ultrasonic powers are quoted as W or otherwise stated.

3. Results and discussion

3.1. Cathode efficiency

Syntheses of Pt nanoparticles were performed at various time managements (χ) between 0.22 and 0.5 in views of optimising the production of Pt nanoparticles with the highest cathode efficiency, η. The total time of the sonoelectrochemical run was set to 60 min. In these experiments no titanium particles arising from cavitational erosion from the ultrasonic horn surface were detected on the filters (see later). The experimental conditions for the sonoelectrochemical investigations, i.e. the process time management parameter (χ) and the cathode efficiency (η) are summarized in Table 1 and Fig. 2.

From the data, it is clearly evident that the cathode efficiency is well over 50% in all applied conditions, particularly exceeding 80% when time management parameter χ is either 0.2875 or 0.375. This is due to the fact that, for low values of χ, t_{ON} is notably lower than t_{US}, i.e. the electrodeposition time is shorter and ultrasonic irradiation lasts longer leading to a few Pt nuclei being formed at the *sonoelectrode* with (a) a large amount of energy being dissipated to the electrolytic solution, (b) an increase in local temperature and (c) redissolution of nanoparticles. Furthermore, from the data, the lowest cathode efficiencies of 59.3% and 67.5% were obtained with t_{US} = 0.5 s which is in good agreement with previous findings [18], according to which longer ultrasonic pulses are detrimental

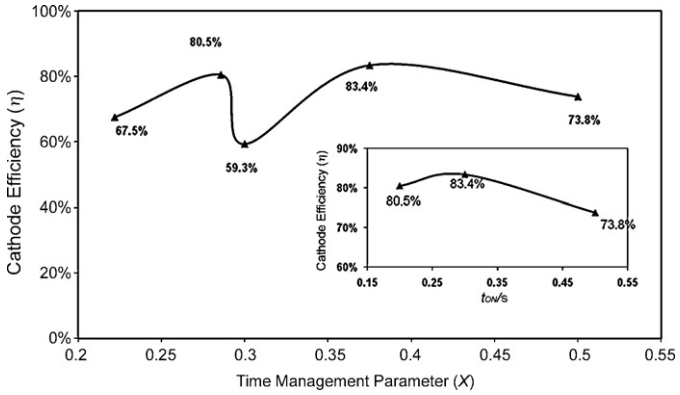

Fig. 2. Cathode efficiency (η) vs. time management parameter (χ) of Pt nanoparticles production. Inset figure: cathode efficiency (η) vs. t_{ON}.

to the formation of nanoparticles in the bulk electrolyte. On the other hand, for larger values of t_{ON}, higher quantity of Pt nuclei was formed on the *sonoelectrode* surface causing water reduction at the nuclei–electrolyte interface due to lower overvoltages. In other words, 'secondary reactions' became predominant and metal reduction hindered. Also, growth of Pt nuclei is promoted by longer electrochemical pulses leading to an increase in Pt nanoparticles mean size causing difficulties in ablating nuclei from the *sonoelectrode* surface, causing a decrease in cathode efficiency (see inset Fig. 2). This observation could explain the low value of process efficiency of χ = 0.3. In fact, the test is characterized of long duration of t_{US} coupled to a longer duration of t_{ON} when compared to Test #1. The two syntheses are both affected by the same decrease of η due to a t_{US} that lasts for 0.5 s, but Test #3 has also a higher t_{ON} which causes a further drop in cathode efficiency.

Fig. 3 shows the dependency of χ with t_{ON} and t_{US}. The figure also shows that as χ increases with t_{ON} the phenomenon is more noticeable when t_{US} is short, while χ decreases, i.e. when $t_{US} \gg t_{ON}$, in particular when t_{ON} is tending to zero. From our observations, the most efficient conditions to produce Pt nanoparticles with high yield are between the two extreme tested values of studied parameters, i.e. with t_{ON} = 0.2–0.3 s and t_{US} = 0.3 s.

Clearly, sonication has the sole role to induce cavitation phenomenon in the electrolytic solution [6,23] and to ablate the metallic nuclei from the cathodic surface. Nuclei formed on the titanium surface during the t_{ON} time are ejected into the electrolyte during t_{US}. Cavitation event takes place and gas bubbles collapse in

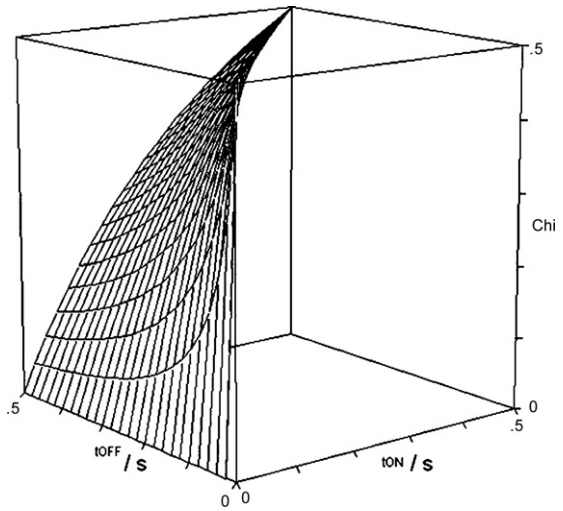

Fig. 3. Cathode efficiency (η) as a function of t_{ON} and t_{US}.

the liquid resulting in high energy release [23–26]. Locally, shock waves propagate through the liquid and generate high-intensity shearing forces causing a displacement of the electrolyte, known as acoustic streaming providing agitation of the solution near the *sonoeletrode*, improving the mass-transport and allowing the system to work under charge transfer control [24].

3.2. Characterization of Pt nanoparticles

Compositional analyses of the filters containing Pt nanoparticles were performed with the aim to rule out any possible contamination from the *sonoelectrode* material or any other bath's components. Analyses were carried out by X-EDS and XRD and showed that all produced nanoparticles were exclusively constituted with platinum and no titanium from the *sonoelectrode* and any other chemicals were detected in tested samples.

However, two other elements (Al and Cu) were detected by EDAX analyses, as shown in Fig. 4(a). Al and Cu peaks are caused by the sample-carrier which is made of Al–Cu alloy, on which Pt nanoparticles were mounted on. XRD measurements [Fig. 4(b)] were performed to investigate the microstructure of Pt nanoparticles. The patterns did not reveal foreign elements other than the characteristic peaks for Pt; this observation indicates that the Pt nanoparticles produced in this study are of high purity. The grain size was calculated from the peak broadening by using the Rietveld method [27,28] and the patterns for the five tests as shown in Fig. 4(b); due to small size effect, the XRD peaks are low and broad.

Spectra revealed the presence of four peaks in each scan. These are typical of a single phase Pt with face centred cubic (*fcc*) structure, according to the JCPDS database (card number 01-1194), where the peaks with 2θ values of 40.08°, 46.58°, 67.92° and 81.59° correspond to the (1 1 1), (2 0 0), (2 2 0) and (3 1 1) planes

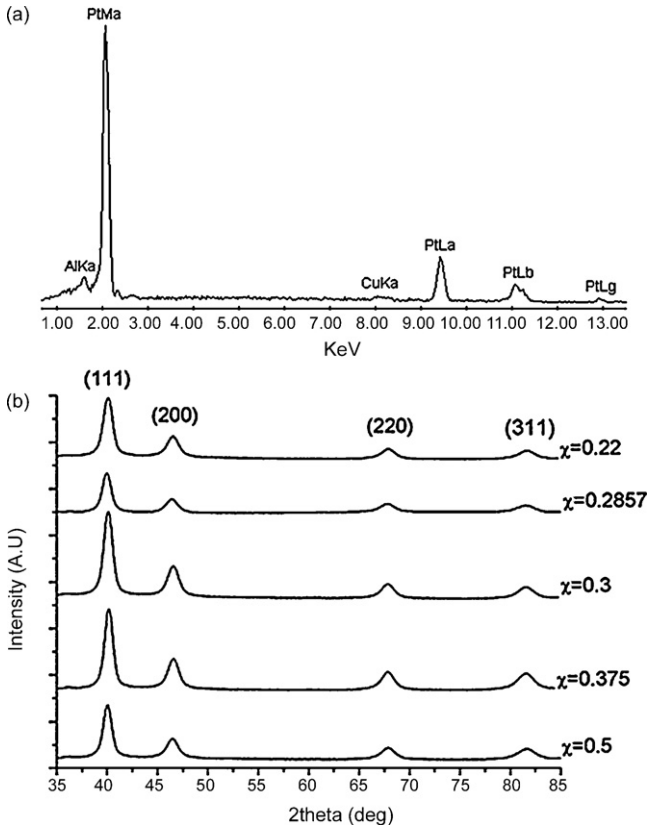

Fig. 4. (a) X-ray energy dispersive spectrometry of Pt nanoparticles and (b) XRD patterns of Pt nanoparticles.

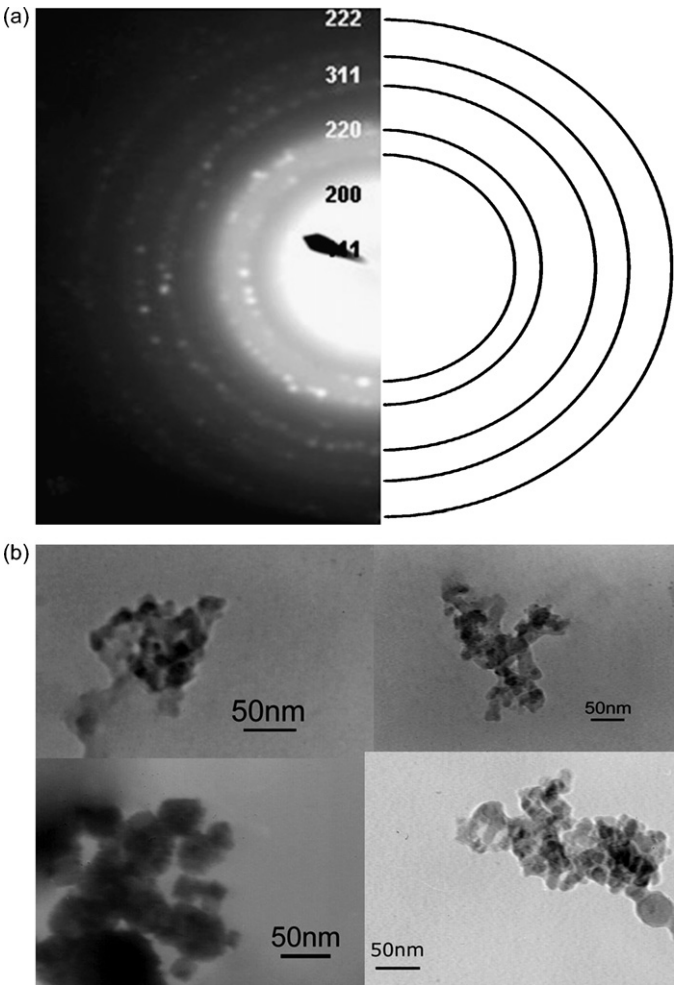

Fig. 5. (a) Selected area electron diffraction pattern of run #1 nanoparticles and (b) TEM images for Test #4.

of the *fcc* Pt phase, respectively [29]. In addition, Pt nanoparticles showed relatively broad peaks, and this feature of the spectra was useful in using the Rietveld method to describe sample microstructure. Furthermore, no signals from other contaminants or Ti-alloy (constituting the *sonoelectrode*) were detected. Once again, this observation shows that, in our conditions, pure Pt nanoparticles can be produced sonoelectrochemically.

Grain size and lattice parameter were calculated for each test and the data are shown in Table 2. The table shows that Pt nanoparticles exhibited a mean grain size ranging from 13 to 15 nm, which is concordant with TEM analyses discussed earlier and measured lattice parameter was in good agreement with the theoretical value obtained from literature of 3.91 Å [30,31].

It can also be emphasized that time management did not affect the microstructural feature of the produced Pt nanopowders, in other words, the samples did not reveal any noticeable variations

Table 2
Structural parameters of Pt nanoparticles obtained from XRD analysis.

Test #	χ	t_{ON}/s	t_{US}/s	a^a/Å	Grain size/nm
1	0.5	0.5	0.3	3.89	13.6
2	0.375	0.3	0.3	3.88	14.3
3	0.3	0.3	0.5	3.88	14.5
4	0.222	0.2	0.5	3.87	13.1
5	0.2857	0.2	0.3	3.90	13.3

[a] Lattice parameter (a).

Table 3
Comparison of interplanar spacings ($d\,h\,k\,l$) with standard data.

Data	JCPDS 01-1194		
d/Å	d/Å	Intensity	$h\,k\,l$
2.26	2.25	100	111
1.93	1.95	30	200
1.44	1.38	16	220
1.21	1.18	16	311
1.06	1.13	3	222

in grain size values and lattice parameters. This means that metal particles can be synthesized with nanometric dimension providing that t_{ON} and t_{US} remain below 0.5 s, i.e. at a maximum χ of 0.5. This finding suggests that under drastic conditions induced by cavitation leading to the "hot spot" mechanism [26,32] do not affect the crystalline structure of Pt nanoparticles.

Fig. 5(a) shows the corresponding selected-area electron diffraction (SAED) pattern, referring to TEM image in Fig. 5(b). It can be indexed to the reflection of a *fcc*-structure which was further confirmed by XRD. The random orientation of the small particles causes the broadening of the diffraction rings. Electron diffraction images were elaborated and the values of interplanar spacing $d_{h\,k\,l}$ were calculated from the diameter of the diffraction rings and compared to the theoretical ones obtained from JCPDS 01-1194 (Table 3) [33–35].

For *fcc* structure, $d_{h\,k\,l} = a/\sqrt{h^2 + k^2 + l^2}$, the lattice parameter (a) can be calculated from measured values for the spacing of the detected planes; for example, for Test 1, a, value measured in TEM-SAED analysis was found to be 3.854 Å which is in good agreement with XRD result and the theoretical data of 2.89 Å.

Morphological characterization was performed by both SEM and TEM. Fig. 5(b) shows a representative TEM micrograph, referring to Pt nanopowders from Test 4. The figure shows that produced Pt nanoparticles are spherical and with minimum diameter of ca. 13 nm with an average size ranging from 10 to 20 nm. For example, it was found that be Pt nanoparticles had mean average size of ca. 14.06 nm with a standard deviation of 2.78 which is in excellent agreement with values obtained from data analysis carried out by XRD characterization [Fig. 6(a)]. Using the Rietveld method, the mean crystallite size was calculated and it was observed that the nanoparticle dimensions were similar suggesting that platinum nanopowders were mono-crystalline rather than poly-crystalline. From the picture it can be seen that nanoparticles have aggregated into secondary particles which are clearly visible in SEM images shown in Fig. 6(b). Globular clusters observed by SEM, and defined as secondary particles, have a mean size ranging between 100 and 200 nm and in turn aggregated and built complex structures; these sphere-chains are the results of the attractive surface tension between the ultra-fine particles, i.e. the high surface energy that leads to agglomeration (in order to minimize system energy).

The difference between TEM and SEM images is due to (a) the low resolution of the SEM compared to TEM and (b) the agglomeration of nanoparticles; in fact during filtration, nanoparticles were compacted on the filter and formed large clusters by weak chemical bonding. These large agglomerates could not be separated before sample preparation leading to an apparent larger particle size on SEM pictures; in other words, one visible particle of 200 nm usually contained several primary nanoparticles of about 15 nm diameter size.

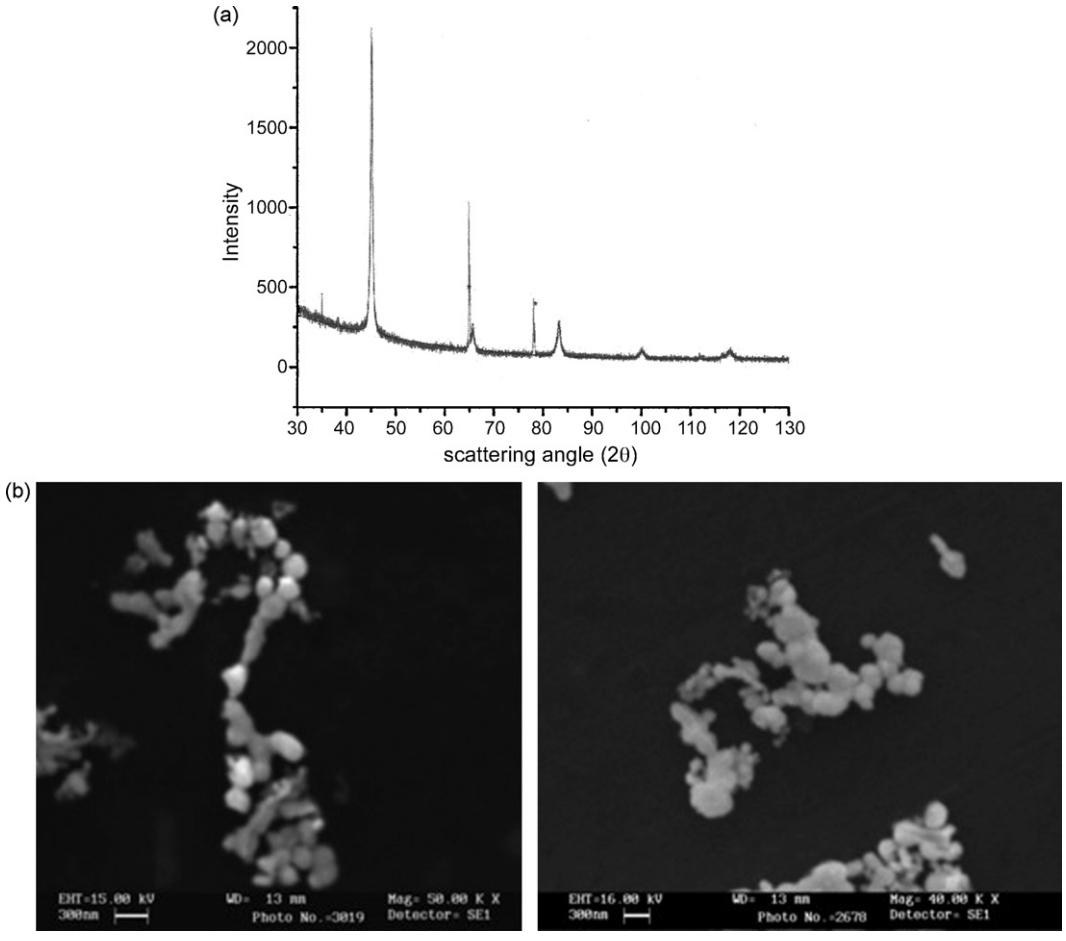

Fig. 6. (a) XRD pattern of Pt nanopowders and (b) SEM micrograph of Pt nanoparticles.

Table 4
Particle sizes and surface areas of Pt nanoparticles showing variation of χ (chi) [the varying process parameter] and η [the cathode efficiency (%)].

Test #	χ	η/%	Particle size/nm	Surface area/$m^2\ g^{-1}$
1	0.222	67.5	10.1	27.76
2	0.2857	80.5	11	25.49
3	0.3	59.3	10.6	26.45
4	0.375	83.4	9.5	29.51
5	0.5	73.8	10.4	26.97

To support these observations, the volume-averaged particle size was calculated from the full width half-maximum of the (1 1 1) peak for various time management parameters (χ) using Fig. 4(b) and the Scherrer equation [36,37]:

$$d\ (\text{Å}) = \frac{k\lambda}{\beta \cos\theta} \tag{4}$$

where d is the average particle size in Å, k is a shape-sensitive coefficient (0.9, assuming spherical spheres), λ the wavelength of radiation used (1.54184 Å), β is the full width half-maximum of the peak in radian and θ is the angle at the position of peak maximum in radian.

Table 4 gives the average particle size for several management parameters (χ) using the Scherrer equation. For a time management parameter of 0.375 corresponding to a cathode efficiency of 83.4%, the lowest average particle size was found to be 11 nm, which is in good agreement with our previous findings.

From, the calculated average particle sizes, it is possible to determine the surface area (SA in $m^2\ g^{-1}$) of platinum, assuming homogeneously distributed and spherical particles, as follows:

$$\text{SA} = \frac{6 \times 1000}{\rho \times d} \tag{5}$$

where ρ is the density of Pt particles (21.4 g cm^{-3}) and d is the average particle size in nm. Table 4 shows the average particle sizes, the surface area, the time management parameter and the cathode efficiency. It was found that from the calculated average Pt particle sizes, surface areas varied between 25 and 30 $m^2\ g^{-1}$ for all the tests indicating that the Pt nanopowders synthesized sonoelectrochemically may be a good candidate for Fuel Cell applications [37]. For example, recently, Liu et al. [37] showed that Pt nanoparticles with surface areas below 65 $m^2\ g^{-1}$ indicated excellent electrocatalytic activities for the O_2 reduction reaction in PEMFC.

4. Conclusions

This paper reports for the first time the production of Pt nanoparticles from aqueous chloroplatinic solutions in the presence of low-frequency high-power ultrasound (20 kHz). It was shown that Pt particles can be synthesized with nanometric dimension providing that t_{ON} and t_{US} remain below 0.5 s with a maximum of process efficiency, χ of 0.5 which exhibited a mean grain size ranging from 11 to 15 nm. SEM and TEM studies showed that globular clusters had a mean size ranging between 100 and 200 nm which in turn aggregated and built complex structures. The morphological and structural studies showed that pure Pt metallic nanoparticles were produced sonoelectrochemically. The smallest produced particles had a mean dimension of about 13 nm, and exhibited a *fcc* structure with a lattice parameter of ca. 3.91 Å. Furthermore, it was observed that sonication enables the production of Pt nanoparticles with high purity, controlled structure and homogenous nanometric crystalline size.

Acknowledgements

The authors would like to thank the European Community Sixth Framework Program through a STREP grant to the SELECT-NANO, Contract No. 516922.03/25/2005 for their kind financial support.

References

[1] N. Moriguchi, J. Chem. Soc. Jpn. 55 (1934) 749.
[2] B.G. Pollet, S.S. Phull, Recent Research Developments in Electrochemistry, Transworld Research Network Publisher, India, 2001, (Chap 4) p. 55.
[3] R. Viennet, V. Ligier, J.-Y. Hihn, D. Bereiziat, P. Nika, M.-L. Doche, Ultrason. Sonochem. 11 (3–4) (2004) 125.
[4] H. Zhang, L.A. Coury, Anal. Chem. 65 (1993) 1552.
[5] R.G. Compton, J.C. Eklund, S.D. Page, G.H.W. Sanders, J. Booth, J. Phys. Chem. 98 (1994) 12410.
[6] R.G. Compton, J.C. Eklund, F. Marken, T.O. Rabbit, R.P. Ackerman's, D.N. Waller, Electrochim. Acta 42 (1997) 2919.
[7] J.P. Lorimer, B. Pollet, S.S. Phull, T.J. Mason, D.J. Walton, Electrochim. Acta 43 (1998) 449.
[8] P.R. Birkin, S. Silva-Martinez, Ultrason. Sonochem. 4 (2) (1997) 121.
[9] P.R. Birkin, H.-M. Hirsimaki, J.G. Frey, T.G. Leighton, Electrochem. Commun. 8 (2006) 1603.
[10] B.G. Pollet, J.-Y. Hihn, M.-L. Doche, J.P. Lorimer, A. Mandroyan, T.J. Mason, J. Electrochem. Soc. 154 (10) (2007) E131.
[11] Z.G. Bai, D.P. Yu, J.J. Wang, Y.H. Zou, W. Qian, J.S. Fu, S.Q. Feng, J. Xu, L.P. You, Mater. Sci. Eng. B 72 (2000) 117.
[12] A. Gedanken, Ultrason. Sonochem. 11 (2004) 47.
[13] J.-M. Qiu, J. Bai, J.-P. Wang, Appl. Phys. Lett. 89 (22) (2006) 222506.
[14] V.R. Stamenkovic, B.S. Mun, M. Arenz, K.J.J. Mayrhofer, C.A. Lucas, G. Wang, P.N. Ross, N.M. Markovic, Nat. Mater. 6 (2007) 241.
[15] R. Ferrando, J. Jellinek, R.L. Johnston, Chem. Rev. 108 (2008) 845.
[16] J. Reisse, H. Francois, J. Vandercammen, O. Fabre, A. Kirsch-de Mesmaeker, C. Maerschalk, J.L. Delplancke, Electrochim. Acta 39 (1) (1994) 37.
[17] J. Reisse, T. Caulier, C. Deckerkheer, O. Fabre, J. Vandercammen, J.L. Delplancke, R. Winand, Ultrason. Sonochem. 3 (1996) S147.
[18] M. Dabalà, B.G. Pollet, V. Zin, E. Campadello, T.J. Mason, J. Appl. Electrochem. 38 (395) (2008) 402.
[19] D.A. Jones, Principles and Prevention of Corrosion, 2nd ed., Macmillan Publishing Company, 1992.
[20] A. Brenner, Electrodeposition of Alloys: Principles and Practices, Academic Press, New York, 1963.
[21] M.A. Margulis, A.N. Malt'sev, Zh. Fiz. Khim. 43 (1969) 1055.
[22] M.A. Margulis, I.M. Margulis, Ultrason. Sonochem. 10 (2003) 343.
[23] J.L. Hardcastle, J.C. Ball, Q. Hong, F. Marken, R.G. Compton, S.D. Bull, S.G. Davies, Ultrason. Sonochem. 7 (1) (2000) 7.
[24] M.E. Hyde, R.G. Compton, J. Electroanal. Chem. 531 (2002) 19.
[25] S.S. Abd El Rehim, A.M. Ibrahim Magdy, M.M. Dankeria, J. Appl. Electrochem. 32 (2002) 1019.
[26] C. Sauter, M.A. Emin, H.P. Schuchmann, S. Tavman, Ultrason. Sonochem. 15 (2008) 517.
[27] R.A. Young (Ed.), The Rietveld Method, International Union of Crystallography, Oxford University Press, Oxford, 1993.
[28] L. Lutterotti, Maud version 2.0: Materials Analysis using Diffraction, 2005 (available via DIALOG) http://www.ing.unitn.it/~maud.
[29] H.P. Klug, L.E. Alexander, X-Ray Diffraction Procedures for Polycrystalline and Amorphous Materials, 2nd ed., Wiley-VCH, 1974.
[30] J.D. Hanawalt, H.W. Rinn, L.K. Frevel, Ind. Eng. Chem. Anal. Ed. 10 (1938) 10475.
[31] International Tables for X-ray Crystallography, vol. IV, Kynoch Press, Birmingham, 1974.
[32] K.S. Suslick, S.B. Choe, A.A. Cichowlas, M.W. Grinstaff, Nature 353 (1991) 414.
[33] J.L. Lábár, Microsc. Microanal. 14 (4) (2008) 287.
[34] J.L. Lábár, Microsc. Microanal. 14 (6.) (2008).
[35] J.L. Làbàr, Process Diffraction version 6.0.4, available via DIALOG, 2002. http://www.mfa.kfki.hu/~labar/ProcDif.htm.
[36] S.P. Jiang, Z. Liu, H.L. Tang, M. Pu, Electrochim. Acta 51 (2006) 5721.
[37] Z. Liu, Z.Q. Tian, S.P. Jiang, Electrochim. Acta 52 (2006) 1213.